
DDoS: A GRAPH NEURAL NETWORK BASED DRUG SYNERGY PREDICTION ALGORITHM

A PREPRINT

Kyriakos Schwarz [✉]

Department of Quantitative Biomedicine
University of Zurich
Schmelzbergstrasse 26, Zurich, CH
kyriakos.schwarz@uzh.ch

Alicia Pliego-Mendieta

Department of Molecular Pathology
University Hospital Zurich
Schmelzbergstrasse 26, Zurich, CH
alicia.pliegomendieta@usz.ch

Lara Planas-Paz

Department of Molecular Pathology
University Hospital Zurich
Schmelzbergstrasse 26, Zurich, CH
lara.planas-paz@usz.ch

Chantal Pauli

Department of Molecular Pathology
University Hospital Zurich
Schmelzbergstrasse 26, Zurich, CH
chantal.pauli@usz.ch

Ahmed Allam [✉]

Department of Quantitative Biomedicine
University of Zurich
Schmelzbergstrasse 26, Zurich, CH
ahmed.allam@uzh.ch

Michael Krauthammer [✉]

Department of Quantitative Biomedicine
University of Zurich
Schmelzbergstrasse 26, Zurich, CH
michael.krauthammer@uzh.ch

October 4, 2022

ABSTRACT

Background Drug synergy occurs when the combined effect of two drugs is greater than the sum of the individual drugs' effect. While cell line data measuring the effect of single drugs are readily available, there is relatively less comparable data on drug synergy given the vast amount of possible drug combinations. Thus, there is interest to use computational approaches to predict drug synergy for untested pairs of drugs.

Methods We introduce a Graph Neural Network (*GNN*) based model for drug synergy prediction, which utilizes drug chemical structures and cell line gene expression data. We use information from the largest drug combination database available (DrugComb), combining drug synergy scores in order to construct high confidence benchmark datasets.

Results Our proposed solution for drug synergy predictions offers a number of benefits: 1) It is trained on high confidence benchmark dataset. 2) It utilizes 34 distinct drug synergy datasets to learn on a wide variety of drugs and cell lines representations. 3) It learns task-specific drug representations, instead of relying on generalized and pre-computed chemical drug features. 4) It achieves similar or better prediction performance (AUPR scores ranging from 0.777 to 0.964) compared to state-of-the-art baseline models when tested on various benchmark datasets.

Conclusions We demonstrate that a *GNN* based model can provide state-of-the-art drug synergy predictions by learning task-specific representations of drugs.

Keywords drug-drug interactions · side effects · genetic variants · cluster analysis · synergy

^{*}Biomedical Informatics, University Hospital of Zurich, Zurich, Switzerland

[†]ETH AI Center, Zurich, Switzerland

Introduction

Treatments targeting complex diseases, such as cancer, frequently lead to acquired drug resistance, due to patient-specific variability. For instance, drugs targeting only one key component of growth or proliferation pathways, may lead to selective pressure and activation of a compensatory mechanism [1], thus making this treatment suboptimal. However, during multi-target inhibition with reduced stringency, drug resistance is less likely. Therefore, the implementation of combination therapy might improve patient treatment as different drugs may target distinct pathways or genes, likely leading to decreased cancer cell survival. In addition to the increased efficacy, combination therapy often reduces toxicity and decreases the likelihood of treatment resistance compared to monotherapy (i.e., single drug) treatments [2].

Due to advancements in high-throughput screening (HTS), the number of drug screening datasets has been growing in recent years. Some examples include the *NCI-ALMANAC* dataset [3] which contains 103 FDA-approved drugs tested in 60 different cell lines (NCI-60) [4] or the large oncology dataset produced by *Merck&Co* [5] which is composed of 38 drugs tested in 39 different cell lines from 6 different tissue types. Furthermore, databases like *DrugComb* [6] have collected and curated drug combination synergy data from 34 different sources, thus comprising 8'397 different drugs, 2'320 cell lines, and 739'964 drug combinations in total.

The availability of larger HTS datasets has enabled model development for improved drug combination synergy predictions. These models utilize genomic information of cells and physiochemical properties of drugs, or drug-cell interactions for the prediction of optimal drug combinations. Commonly used models include RandomForest, SupportVectorMachine, GradientBoostingMachine, and NaiveBayes [7]. However, more recently Deep Learning based models have demonstrated to be advantageous at managing large amounts of data and learning useful representations that often lead to an improved prediction performance. For instance, *DeepSynergy* [8], a feed-forward neural network (*FFNN*) with tanh normalization outperformed previous models. *DeepSynergy* utilized the *Merck* dataset, combining gene expression data, HTS data and drug chemical information. Furthermore, *AuDNNsynergy* [9] employed three autoencoders in order to utilize copy number variation data (CNV), mutations and gene expression, likewise on the *Merck* dataset. *MatchMaker* [10], a deep neural network, feeds gene expression and drug chemical features from the *DrugComb* database into separate drug specific subnetworks and, subsequently, into a synergy prediction network.

A variety of additional algorithms have been developed for drug synergy predictions. However, these models come with several limitations: 1) Multiple synergy scoring methods have been developed, though each one has its biases and drawbacks. Yet, the majority of studies rely only on one synergy score, i.e., Loewe or Bliss, thus making them biased in respect to the assumptions of the synergy score that they are using [11]. 2) Most prediction models only utilize a single dataset, which limits the number of drug and cell line combinations a model learns on. Additionally, this also limits the extent to which the model can be generalized to unknown drugs and unutilized cell lines. 3) Commonly, existing models take advantage of pre-computed chemical properties of drugs. Though, with the wider adaption of Graph Neural Networks (*GNNs*) in recent years it has become more advantageous to learn task specific representations of drugs in the form of graphs (i.e., chemical structures where atoms are nodes and bonds are edges).

To this end, we propose a Graph Neural Network (*GNN*) based model, *DDoS* (**D**rug-**D**rug combination **S**ynergy model), which offers multiple advantages: 1) It utilizes four different drug synergy scores (Loewe, Bliss, HSA, ZIP), as well as three distinct majority voting based combinations of those four scores. Hence, it is trained on binary labels with much higher confidence of synergy compared to single score based labels. 2) It includes samples from *DrugComb*, which is a collection of 34 distinct drug synergy datasets, in order to learn on a wide variety of drugs and cell lines. 3) It learns task-specific drug representations, instead of relying on generalized pre-computed chemical features of drugs. 4) It outperforms state-of-the-art baseline models when tested on seven distinct benchmark datasets.

Methods

Obtained datasets

We obtained the drug combination dataset from the *DrugComb* [6] database (version 1.5 - <https://drugcomb.org/>). This dataset initially contains 1'432'351 samples (i.e., *Drug A*, *Drug B*, *Cell Line* combination triplets). These samples have originated from 34 distinct studies, including, for instance, *NCI-ALMANAC* [3], *O'NEIL (Merck)* [12] and *CLOUD* [13] among them. For each of the samples we utilized the chemical structures of the drugs, the gene expression profiles of untreated cell lines, and four different synergy scores (Loewe, Bliss, HSA, ZIP).

Chemical features

For each drug in the *DrugComb* database a chemical representation string (SMILES) was included. Through the *RDKit* cheminformatics software package [14] we then extracted the following features for each atom of the chemical structure of a drug:

1) Atomic number: Number of protons found in the nucleus of this atom. 2) Chirality (chiral tag): Whether they are superimposable on their mirror image or not. 3) Degree of the atom in the molecule including Hs (hydrogen atoms). The degree of an atom is defined to be its number of directly-bonded neighbors. The degree is independent of bond orders. 4) Formal charge. 5) Total number of Hs (explicit and implicit) on the atom. 6) Number of radical electrons. 7) Hybridization of the atom. 8) Whether the atom is aromatic or not. 9) Whether the atom is in ring or not.

Therefore, for a given chemical structure of a drug with R atoms we constructed a $R \times 9$ feature matrix, where R is the number of atoms (nodes) of the chemical structure graph.

Additionally, we constructed for each drug an $R \times R$ binary adjacency matrix A , which contained the structural information of each chemical compound. Particularly, this matrix has a value of 1 at each position where two atoms are forming a bond, otherwise it is 0s.

Gene Expression features

For this study we retrieved untreated cell line features from https://www.cancerrxgene.org/gdsc1000/GDSC1000_WebResources/Data/preprocessed/Cell_line_RMA_proc_basalExp.txt.zip. This includes the RMA normalised basal expression profiles for all the cell lines included in the raw data by [15], which contains transcriptional profiles of roughly 1'000 human cancer cell lines (E - MTAB-3610 in *ArrayExpress*). For each cell line the normalized expression levels of 17'737 genes were included, out of which we selected $l' = 908$ landmark genes. The latter were accessed from the L1000 [16] project (<https://clue.io/>). Hence, each cell line is represented by a feature vector of length 908. See Supplementary Files for all included genes.

Drug synergy reference scores

Drug synergy refers to a quantification of drug interaction [17], i.e., how much excess drug response (e.g., tumor cell death) is observed compared to the expectation (that is, no excess). Thus, the reference synergy scores (Loewe, Bliss, HSA, ZIP) provide a percentage of excess response, or reduced response in the antagonistic setting.

Loewe Additivity Model

The Loewe additivity model is based on the concepts of sham combination and dose equivalence. Ergo, the expected effect y_{Loewe} can be defined as if a drug was combined with itself, i.e., $y_{Loewe} = y_1(x_1 + x_2) = y_2(x_1 + x_2)$, where y_1 and y_2 indicate the drug responses of drug 1 and drug 2, respectively. This model considers the dose-response curves of individual drugs, where the expected effect must satisfy:

$$\frac{x_1}{x_{Loewe}^1} + \frac{x_2}{x_{Loewe}^2} = 1, \quad (1)$$

where x_1, x_2 are drug doses and x_{Loewe}^1, x_{Loewe}^2 are the doses of drug 1 and 2 alone that produce y_{Loewe} . By using 4-parameter log-logistic (4PL) curves to describe dose-response curves the following parametric form of previous equation is derived:

$$\frac{x_1}{m_1 \left(\frac{y_{Loewe} - E_{min}^1}{E_{max}^1 - y_{Loewe}} \right)^{\lambda_1}} + \frac{x_2}{m_2 \left(\frac{y_{Loewe} - E_{min}^2}{E_{max}^2 - y_{Loewe}} \right)^{\lambda_2}} = 1, \quad (2)$$

where $E_{\min}, E_{\max} \in [0, 1]$ are minimal and maximal effects of the drug, m_1, m_2 are the doses of the drug that produce the midpoint effect of $E_{\min} + E_{\max}$, also known as relative EC_{50} or IC_{50} , and $\lambda_1 (\lambda_1 > 0), \lambda_2 (\lambda_2 > 0)$ are the shape parameters indicating the sigmoidicity or slope of dose-response curves. A numerical nonlinear solver can be then used to determine y_{Loewe} for (x_1, x_2) .

Bliss independence model

The Bliss independence model is based on a stochastic process. It assumes that each drug has different response in a particular scenario and that they elicit their effects independently. Therefore, the combination response is based on the probability of those independent events. Hence, the Bliss score formula is as follows:

$$y_{Bliss} = y_1 + y_2 - y_1 y_2, \quad (3)$$

where y_{Bliss} represents the Bliss response. y_1 and y_2 indicate the drug responses of drug 1 (D_1) and drug 2 (D_2), respectively.

Highest Single Agent Model

The highest single agent model (HSA) states that the effect of the expected combination effect is equal to the maximum effect of each individual drug at specific concentrations. Thus, the formula representing the model is:

$$y_{HSA} = \max(y_1, y_2), \quad (4)$$

where y_1 and y_2 are the monotherapy (single drug) effect of drug 1 (D_1) and drug 2 (D_2), respectively.

Zero Interaction Potency (ZIP)

The Zero Interaction Potency calculates the expected effect of two drugs under the assumption that they do not potentiate each other, i.e., both assumptions of the Loewe model and the Bliss model are met:

$$y_{ZIP} = \frac{\left(\frac{x_1}{m_1}\right)^{\lambda_1}}{1 + \left(\frac{x_1}{m_1}\right)^{\lambda_1}} + \frac{\left(\frac{x_2}{m_2}\right)^{\lambda_2}}{1 + \left(\frac{x_2}{m_2}\right)^{\lambda_2}} - \frac{\left(\frac{x_1}{m_1}\right)^{\lambda_1}}{1 + \left(\frac{x_1}{m_1}\right)^{\lambda_1}} \frac{\left(\frac{x_2}{m_2}\right)^{\lambda_2}}{1 + \left(\frac{x_2}{m_2}\right)^{\lambda_2}}, \quad (5)$$

where $x_1, x_2, m_1, m_2, \lambda_1$ and λ_2 , are defined in the Loewe model section.

Benchmark datasets

The initial dataset of 1'432'351 samples was processed as in the following steps: We first selected the triplets (*Drug A, Drug B, Cell Line* combinations) which had a corresponding cell line identifier in the gene expression features table (RMA data above). Additionally, we filtered out samples which had missing values in either identifiers (drug name or cell line) or missing synergy scores. We furthermore filtered out duplicated triplets.

Subsequently, for each of the synergy scores (Loewe, Bliss, HSA, ZIP) we defined positive (synergistic) and negative (antagonistic) samples based on thresholding. As the synergy scores included in *DrugComb* were calculated using the *SynergyFinder* software [18], we utilized the thresholds provided in their documentation³. The recommended thresholds (≥ 10 for synergy, and ≤ -10 for antagonism classes) were applied on the four synergy scores individually.

However, each of the synergy scores comes with its biases and limitations, as they are calculated under different assumptions. For instance, the Loewe synergy score, which assumes the *Dose Equivalence Principle* (DEP framework), is known to artificially increase synergy scores due to a Hill-slope dependent bias [11]. Therefore, we also constructed three additional majority-voting datasets based on the previous four, where for each majority voting dataset we included samples in their positives (and respectively negatives) in case at least 2, 3 or all 4 thresholded scores (from Loewe, Bliss, HSA, ZIP) also include those samples in their respective positives or negatives. Hence, the three additional datasets provided with higher confidence of synergy or antagonism than those provided by each synergy score, separately. Hence, seven distinct datasets were resulted which we utilized for model training and evaluation, as listed in Table 1.

³https://synergyfinder.fimm.fi/synergy/synfin_docs/#datanal

Dataset	# Samples	% Positive Labels	# Drugs	# Cell Lines
Loewe	166'608	~ 15	2'148	169
Bliss	126'619	~ 49	1'869	169
HSA	109'691	~ 30	1'190	167
ZIP	89'868	~ 40	1'811	167
Majority (4)	26'031	~ 50	895	153
Majority (3)	64'168	~ 36	987	163
Majority (2)	110'340	~ 40	1'673	167

Table 1: Benchmark datasets.

Model outcome task

The prediction task in our seven constructed datasets is binary classification (i.e. **synergistic** or **antagonistic**). The input samples of the model are drug-drug-cell line triplets, which consist of two chemical feature matrices, two adjacency matrices (as defined above), respectively, for each drug, and a gene expression feature vector representing the cell line of each sample. A sample-specific probability distribution for the two labels/classes (synergistic and antagonistic) is generated by the model as output.

DDoS: architecture description

Our proposed drug synergy architecture, *DDoS* (see Figure 1), consists of three parts:

1. A Graph Neural Network (*GNN*) model for calculating drug feature representation vectors.
2. A *Gene Rescaling* model for rescaling gene expression features, in order to optimize gene features representation.
3. A Classifier model (feed-forward neural network followed by a LogSoftmax function) to compute a probability distribution over the two classes using the concatenated outputs (learned representation vectors) of the *GNN* and *Gene Rescaling* models.

Graph Neural Network model

In this work, we represent drugs as graphs based on their chemical structures, where atoms are represented as set of nodes $V = \{1, \dots, A\}$ and bonds as edges $E \subseteq V \times V$ in a drug graph $G = (V, E)$. Like feed-forward networks, the *GNN* model consists of multiple layers, L , which signifies the "depth" of the network. Particularly, a layer $l \in \{1, \dots, L\}$ can be viewed as the l -hop neighborhood of a node (atom), i.e., the subgraph of all atoms reachable within l steps.

Node representation: Every node (atom) $i \in V$ is initially represented by a vector $h_i^{(l)} \in \mathbb{R}^9$, at layer l , and its neighbors are defined by $N_i = \{j \in V \mid (j, i) \in E\}$. The representation of each node (h_i) is updated at layer $l + 1$ by the aggregation of the representations of its neighbors:

$$h_i^{(l+1)} = \phi(\xi(\{h_j^{(l)} \mid j \in N_i\})), \tag{6}$$

where ϕ, ξ are differentiable functions and ξ is permutation invariant (i.e., generally order invariant).

Specifically, we utilize the GATv2 operator [19] for updating each h_i (see Equation 7). This operator provides two advantages, compared to the more commonly used implementation of GAT [20]: 1) the aggregation (ξ) of the neighbors $j \in N_i$ is based on the weighted average of learned weights (using attention) instead of treating all neighbors with equal importance, and 2) every node can attend to any other node (dynamic attention) while the original GAT is limited to static attention.

$$h_i^{(l+1)} = \phi(\alpha_{i,i} \Theta \mathbf{h}_i^{(l)} + \sum_{j \in \mathcal{N}_i} \alpha_{i,j} \Theta \mathbf{h}_j^{(l)}), \tag{7}$$

where the attention coefficients $\alpha_{i,j}$ are computed as:

$$\alpha_{i,j} = \frac{\exp\left(\mathbf{a}^\top \text{LeakyReLU}\left(\Theta[\mathbf{h}_i^{(l)} \parallel \mathbf{h}_j^{(l)}]\right)\right)}{\sum_{k \in \mathcal{N}_i \cup \{i\}} \exp\left(\mathbf{a}^\top \text{LeakyReLU}\left(\Theta[\mathbf{h}_i^{(l)} \parallel \mathbf{h}_k^{(l)}]\right)\right)}, \quad (8)$$

\mathbf{a}, Θ are learned parameters and ϕ is the *ELU* activation function.

Graph representation: Subsequently, layer-specific graph representations $g^{(l)}$ are generated by aggregating (i.e., global mean pooling) the updated node representations $h_i^{(l)}$:

$$g^{(l)} = \frac{1}{A} \sum_{n=1}^A h_n^{(l)}, \quad (9)$$

where the number of *GNN* layers L is a hyperparameter. Finally, the weighted average z of the graph representations $\{g^{(0)}, \dots, g^{(L)}\}$ is computed by computing the attention weights between each two graph representations, parameterized by a global context vector c with learnable parameters (see Equations 10, 11, 12).

$$\psi^l = \frac{\exp(\text{score}(c, g^l))}{\sum_{j=1}^L \exp(\text{score}(c, g^j))} \quad (10)$$

$$\text{score}(c, g^l) = \frac{c^\top g^l}{\sqrt{d'}} \quad (11)$$

$$z = \sum_{l=1}^L \psi^l g^l \quad (12)$$

where d' is the embedding dimension of g^l (graph's learned representation at layer l).

Therefore, for each *Drug A* and *Drug B* in an input sample triplet, two separate drug representation vectors are computed, z_a and z_b , respectively.

Gene Rescaling Model

The *Gene Rescaling* model utilizes a learnable scalar in order to apply it to each gene on the gene expression feature vector of each sample triplet (*Drug A*, *Drug B*, *Cell Line*). For this purpose, a global context vector, r , is utilized whose parameters are optimized during training. Given a gene expression vector, $u_e = \{e_1, e_2, \dots, e_T\}$, with T number of genes, it computes scores $\zeta_t \forall t \in [1, \dots, T]$ by calculating the pairwise similarity between the context vector r and the set u_e (Eq. 13, 14). Subsequently, these scores are normalized (by Softmax) in order to generate a new gene vector representation z_e with the same length T by calculating the weighted sum of the $\{e_1, e_2, \dots, e_T\}$ vectors (Eq. 15). Finally, z_e is concatenated with the drug feature representation vectors, z_a and z_b , and fed into the classifier layer.

$$\zeta_t = \frac{\exp(\text{score}(r, e_t))}{\sum_{j=1}^T \exp(\text{score}(r, e_j))} \quad (13)$$

$$\text{score}(r, e_t) = \frac{r^\top e_t}{\sqrt{l'}} \quad (14)$$

$$z_e = \sum_{t=1}^T \zeta_t e_t \quad (15)$$

where l' is the number of selected *landmark* genes (i.e. 908).

Classifier Model

The *Drug A* and *Drug B* feature representation vectors (z_a, z_b) computed by the *GNN* model, along with the rescaled gene expression feature vector (z_e) computed by the *Gene Rescaling* model, are concatenated together to form a unified representation. Subsequently, this concatenated vector is fed into the Classifier model, which consists of a feed-forward neural network (*FFNN*). The *FFNN* contains two hidden layers, whose sizes are determined by hyperparameters, and uses the *ReLU* non-linear activation function and dropout for regularization. The output layer generates a vector of two elements which is passed to a *LogSoftmax* function to obtain a log probability distribution over whether a sample (triplet) is more likely to be synergistic or not.

Objective Function

With a total of M samples (*Drug A*, *Drug B*, *Cell Line* triplets), the loss of the m -th sample ($m \in \{1, \dots, M\}$) is computed using the negative log-likelihood (*NLL*) loss, L^{NLL} (equivalent to binary cross-entropy). For each m -th sample, the loss is calculated based on its true label y_m and corresponding predicted probability \hat{y}_m , where $y_m \in \{0, 1\}$:

$$l_{(m)}^{\text{NLL}} = -[y_{(m)} \log \hat{y}_{(m)} + (1 - y_{(m)}) \log(1 - \hat{y}_{(m)})] \quad (16)$$

Accordingly, the total loss L^{NLL} is computed as:

$$L^{\text{NLL}} = \frac{1}{M} \sum_{i=1}^M l_{(m)}^{\text{NLL}} \quad (17)$$

For model training, we utilized a *GNN*-specific form of mini-batching, in which graph adjacency matrices are stacked in a diagonal fashion. This creates a giant graph which contains multiple isolated subgraphs. In our graph-based setting, common mini-batching approaches would be suboptimal, as they would likely result in unnecessary memory consumption. During training the L^{NLL} loss is computed and the model weights are updated based on processing each mini-batch of the training set.

Baseline models

We employed several baseline models for comparison to our proposed model *DDoS*, with a special focus on the *DeepSynergy* [8] state-of-the-art model and a vanilla *GNN* based model. *DeepSynergy* is a feed-forward neural network which utilizes the concatenated drug and cell line feature vectors as input and generates a predicted synergy score in its output layer. We replicated this model architecture in *PyTorch* as closely as possible in order to utilize it for comparison. Furthermore, we implemented a baseline *GNN*-based model which employs the commonly utilized *GAT* operator. We additionally included four baseline models from the *scikit-learn* machine learning library [21], i.e., *GradientBoostingClassifier*, *KNeighborsClassifier*, *DecisionTreeClassifier* and *LogisticRegression* for further model performance comparisons.

Model evaluation

We evaluated models performance on the seven processed datasets (four given synergy scores and three combined majority voting scores). For this evaluation we used standard binary classification metrics, i.e. *AUC* and *AUPR*. *AUC* is the Area Under the True Positive Rate-False Positive Rate Curve, while *AUPR* is the Area Under the Precision-Recall Curve. While most datasets we evaluated are fairly balanced (see Table 1), the "Loewe" dataset only has $\sim 15\%$ positive (synergistic) labels. When such class imbalances are prevalent then the *AUPR* evaluation score is considered to be a fairer measure.

Training workflow

Our models were trained with a 5-fold cross-validation strategy. Additionally, 10% of the training partition of each fold was reserved for validation and hyperparameter tuning. We initially selected random hyperparameter values for the training of each model on a random fold (out of 5 folds). Subsequently, we repeated the training of each model on all 5 folds based on the best performing hyperparameters of the initial random fold. Finally, the trained models (on all 5 folds) were tested on the test split. Thus, we computed *AUPR* and *AUC* performance scores for all 7 datasets (Loewe, Bliss, HSA, ZIP, Majority (4), Majority (3), Majority (2)).

The hyperparameters we utilized for the training of all models, are: Batch size: 300, Epochs: 100, Graph embedding dimension: 100, Number of *GNN* layers (L): 5, Dropout: 0.3, Learning rate: 0.0003, Weight decay: 0.0, Hidden layer 1 size: 4096, Hidden layer 2 size: 1024.

For our experiments, we developed our code that built upon the following software packages: *Python* (v. 3.9.9), *PyG* (v. 2.0.3) [22], *PyTorch* (v. 1.9.1) [23], *scikit-learn* (v. 1.0.2) [21], *Open Graph Benchmark* (v. 1.3.2) [24], *Strategies for Pre-training Graph Neural Networks* repository [25], and *RDKit* (v. 2021.09.3) [14].

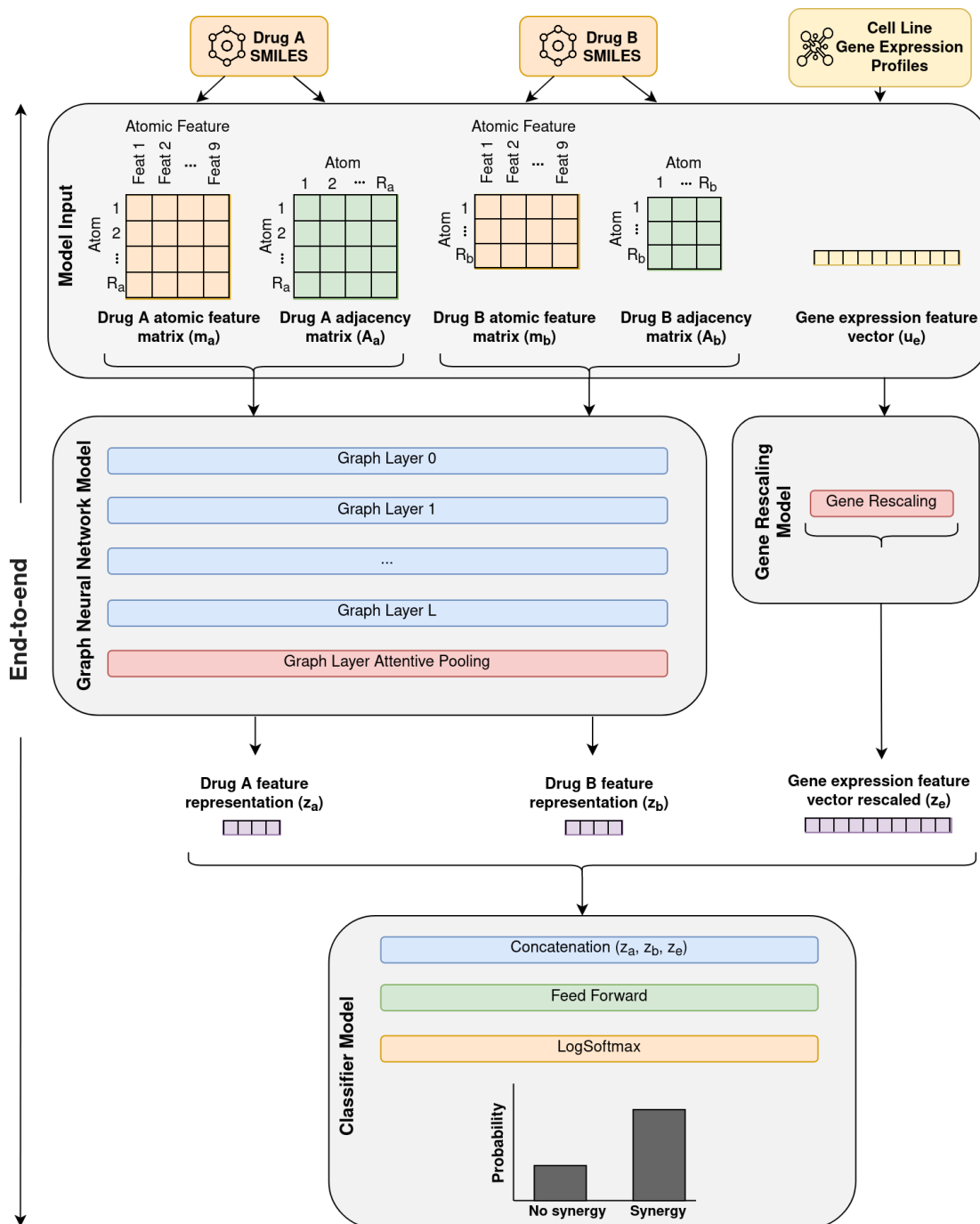


Figure 1: *DDoS* model architecture. 1) The model accepts samples of triplets (*Drug A*, *Drug B*, *Cell Line Gene Expression*) represented by two atomic feature matrices (m_a , m_b), two adjacency matrices (A_a , A_b), and one gene expression vector, u_e . Each drug in a sample is represented by a matrix containing atomic features in separate rows. Each gene expression vector contains gene expression measurements for 908 distinct *landmark* genes. 2) The atomic feature matrix and the adjacency matrix of each drug are fed into a *GNN* model, for each drug separately, in order to learn drug feature representations, z_a and z_b , respectively. The gene expression features are rescaled by the *Gene Rescaling* model, resulting in a representation vector z_e . 3) The vectors z_a , z_b and z_e are concatenated and fed into a feed-forward neural network (*FFNN*), which maps the concatenated vector to an output layer of size two (i.e., as the number of classes). A LogSoftmax function is applied on the *FFNN* output to compute a log probability distribution, i.e., whether a sample is more likely synergistic or antagonistic.

Results

Model evaluation results

Our *DDoS* model was compared to six baseline models, including a state-of-the-art architecture, DeepSynergy. As shown in Table 2, our model vastly outperforms the baseline models. We tested the model performances on seven derived datasets, four of which are based on individual drug synergy scores and three with combined scores.

When compared to the state-of-the-art baseline model, DeepSynergy, our model has better performance on all seven datasets in both AUPR and AUC scores. Compared to DeepSynergy model, for the Majority-4 dataset, our model has a AUPR score of 0.964 vs. 0.854 and AUC score of 0.973 vs. 0.889. Similarly, for the Majority-3 dataset: AUPR 0.963 vs. 0.825, AUC 0.978 vs. 0.889, for the Majority-2 dataset: AUPR 0.953 vs. 0.807, AUC 0.968 vs. 0.867, for the ZIP dataset: AUPR 0.948 vs. 0.859, AUC 0.950 vs. 0.864, for the Loewe dataset: AUPR 0.777 vs. 0.544, AUC 0.929 vs. 0.836, for the Bliss dataset: AUPR 0.930 vs. 0.807, AUC 0.951 vs. 0.849, and for the HSA dataset: AUPR 0.921 vs. 0.789, AUC 0.956 vs. 0.874. Furthermore, comparing our model to non-graph based baseline models, we observed similar and larger gap (i.e., difference in scores) using both metrics (AUPR and AUC). Lastly, our model still outperforms a GNN-based model (*GNN-GAT*) on all seven datasets in both AUC and AUPR scores (Table 2). The difference in performance ranges from 3 to 18 points in AUPR, and from 3 to 6 points in AUC scores respectively favoring our model.

For further model evaluation, we generated four additional benchmark datasets, one for each of the four synergy scores (Loewe, Bliss, HSA, ZIP). These datasets differ from the reported benchmark dataset above, by including the additive triplets in their respective non-synergistic class (negative class), i.e., triplets which have synergy values between the two specified thresholds, -10 and 10 (see *Benchmark datasets* section for more details). Those datasets are vastly more imbalanced, since the new non-synergistic class includes a large number of additional samples. Therefore, those resulting Loewe, Bliss, HSA and ZIP datasets include 5.3%, 13.8%, 6.5% and 11.9% positive (synergistic) labels, respectively. This imbalance would be challenging for models’ performance when using AUPR metric.

Our model still outperforms the DeepSynergy baseline model on those four additional datasets as reported in Table 3. For the ZIP dataset our model has a AUPR score of 0.795 vs. 0.574 and AUC score of 0.951 vs. 0.891 for the DeepSynergy model. Similarly, for the Loewe dataset: AUPR 0.406 vs. 0.235, AUC 0.900 vs. 0.835, for the Bliss dataset: AUPR 0.824 vs. 0.587, AUC 0.948 vs. 0.878 and lastly for the HSA dataset: AUPR 0.522 vs. 0.297, AUC 0.915 vs. 0.829. Hence, our model outperforms the baseline model even when trained on datasets with large class imbalances.

Model	Majority-4		Majority-3		Majority-2		ZIP		Loewe		Bliss		HSA	
	AUPR	AUC	AUPR	AUC	AUPR	AUC	AUPR	AUC	AUPR	AUC	AUPR	AUC	AUPR	AUC
GNN-DDoS (ours)	0.964	0.973	0.963	0.978	0.953	0.968	0.948	0.950	0.777	0.929	0.930	0.951	0.921	0.956
GNN-GAT	0.932	0.947	0.917	0.948	0.903	0.933	0.914	0.918	0.597	0.861	0.886	0.915	0.865	0.921
DeepSynergy	0.854	0.889	0.825	0.889	0.807	0.867	0.859	0.864	0.544	0.836	0.807	0.849	0.789	0.874
Logistic Regression	0.703	0.745	0.593	0.697	0.575	0.664	0.690	0.671	0.371	0.748	0.611	0.656	0.607	0.718
Decision Tree	0.837	0.821	0.792	0.800	0.770	0.765	0.836	0.763	0.567	0.718	0.785	0.749	0.732	0.766
KNN	0.845	0.874	0.806	0.866	0.771	0.826	0.845	0.830	0.524	0.789	0.775	0.808	0.746	0.836
Gradient Boosting	0.844	0.877	0.751	0.830	0.701	0.777	0.784	0.780	0.510	0.817	0.707	0.752	0.709	0.810

Table 2: Model evaluation scores for the main datasets.

Model	ZIP		Loewe		Bliss		HSA	
	AUPR	AUC	AUPR	AUC	AUPR	AUC	AUPR	AUC
GNN-DDoS (ours)	0.795	0.951	0.406	0.900	0.824	0.948	0.522	0.915
DeepSynergy	0.574	0.891	0.235	0.835	0.587	0.878	0.297	0.829

Table 3: Model evaluation scores for the additional datasets, including additive samples.

Case Studies

As to further validate the competency of our model, we examined the top 20 novel synergistic predictions of drug-drug-cell line combinations, ranked by the highest synergy probability from our model, *DDoS*. For consistency with previous studies, we considered the top "false positives" of the Loewe dataset and investigated how strongly these predictions are supported by the remaining synergy scores, i.e., Bliss, ZIP and HSA. In Table 4 we list those triplets along with an indication of how many of the three scores have a positive interaction score for each triplet. We discovered that 75% of the top triplets have at least one other synergy score (Bliss, ZIP, HSA) supporting those predictions while in nearly 50% of the cases all three scores have this indication, highlighting the efficacy of our model.

Rank	Drug A	Drug B	Cell Line	Indication
1	Erlotinib	7-ethyl-10-hydroxycamptothecin	NCIH520	***
2	Dimesna	Temozolomide	T98G	-
3	Crizotinib	Actinomycin d	SK-MEL-2	-
4	Uramustine	Actinomycin d	M14	-
5	391210-10-9	Deforolimus	OCUBM	***
6	Crizotinib	Mithramycin	SK-MEL-2	***
7	Sunitinib	891494-63-6	NCIH2122	***
8	Geldanamycin	915019-65-7	OCUBM	***
9	Foscarnet sodium	Temozolomide	T98G	-
10	Vemurafenib	Mithramycin	RPMI-8226	***
11	Paclitaxel	Lapatinib	RPMI7951	***
12	Actinomycin d	Antibiotic ad 32	M14	***
13	Geldanamycin	Topotecan	A375	-
14	Crenolanib	Ncgc00162423-03	L-1236	**
15	Antibiotic ay 22989	Adm hydrochloride	KM12	**
16	Docetaxel	Lenalidomide	RVH-421	**
17	Docetaxel	Zm 336372	WM115	***
18	1032350-13-2	Nilutamide	SK-MEL-28	**
19	Cyclophosphamide	Temozolomide	T-47D	**
20	Vandetanib	Mithramycin	HL-60(TB)	*

Table 4: Case studies - Top 20 "false positive" predictions of the Loewe dataset, ranked by the model probability of synergistic outcome. The number of * indicate how many of the HSA, ZIP and Bliss scores support each prediction.

Discussion

Learned representations

Our drug synergy prediction model, *DDoS*, makes use of an *end-to-end* architecture, in order to learn task-specific drug and cell line representations. Antithetically, the majority of previous solutions are utilizing task-agnostic, pre-computed chemical characteristics of drugs ([8], [9], [10]), in addition to suboptimal representations of gene expression features. We learn task-specific drug chemical representations through a *GNN*-based model and the gene expression vectors are optimally rescaled during model training. This approach showed to be advantageous based on the improved performance of our model, *DDoS* in our reported experiments.

Drug synergy scores

For model training we utilized data from a large drug combination database which contains nearly 1.5M drug-drug-cell line combination triplets and four distinct drug synergy scores. Conversely, the baseline model, DeepSynergy, was originally trained only on 23'062 samples [8]. Thus, our model was able to learn from the most complete drug combination dataset to date, including thousands of drugs and hundreds of cell lines.

Moreover, due to the different underlying assumptions of drug synergy scores, each score includes its distinct biases and limitations. This leads to multiple different labels (synergistic or not) assigned to the same samples, depending on which synergy score is utilized. Thus, only a fraction of samples are characterised as synergistic by all four scores simultaneously (see Majority-4 dataset in Table 1). By combining these scores through majority voting, we constructed and trained on three high-confidence datasets in addition to the four individual drug synergy scores.

Limitations

Despite the multiple advantages, our solution also encompasses some limitations. The cell line features we utilized are only based on gene expression data. For a more informative representation further cell line characteristics can be included, e.g., mutations, copy number variations, pathways, drug targets, and more. Additionally, majority voting based combinations of synergy scores alleviate some of the biases of each individual score. Ideally, improved single drug synergy scores would provide these advantages. More recently developed synergy scores, as for instance *MuSyC* [11], might provide such benefits. Furthermore, the model classification task (synergistic vs. non-synergistic) could be expanded, in order to include further classes, as for example to additionally make predictions on the efficacy and potential toxic effects of drug combinations. Finally, most drugs and cell lines included in the dataset concern cancer treatments. Accordingly, an inclusion of experiments for other types of complex diseases (e.g., viral infections), would reduce this cancer-specific disease bias of our model.

Conclusions

We introduced *DDoS*, a *GNN*-based deep learning model to predict drug synergy that might be helpful for identifying combination therapy in treating complex diseases. We trained our model on samples from the largest drug combination database *DrugComb* (comprised of 34 distinct datasets), and constructed high-confidence training labels based on the common four drug synergy scores used in the literature. In conclusion, our model outperformed state-of-the-art baseline models in drug synergy prediction. Identification of synergistic effects between approved drugs is of clinical relevance as drug repurposing may reduce the costly, slow and often unsuccessful development of new drugs that fail to show efficacy in clinical trials even after extensive preclinical safety testing. In the future, complementing *in silico* drug synergy discovery with *ex vivo* testing of selected combinations of anti-cancer drugs in relevant patient-derived 3D organoid models may greatly impact the clinical translatability of this approach.

Availability of data and materials

The preprocessing scripts and the models' implementation (training and testing) workflow is made publicly available at <https://github.com/uzh-dqbm-cmi/graphnn>

Competing interests

The authors declare that they have no competing interests.

Acknowledgements

NA

Author's contributions

KS and APM worked on the development of processing and analysis workflow. KS implemented the algorithms and models. KS and APM analyzed and interpreted the data. KS and APM drafted the manuscript. MK, AA, CP and LPP supervised the project and edited the manuscript. All authors approved the final article.

Acronyms

AUC	Area under Receiver Operating Characteristics curve
AUPR	Area under Precision-Recall curve
CNV	Copy number variation
DDoS	Drug-drug synergy
FDA	Food and drug administration
FFNN	Feed-forward neural network
GAT	Graph attention network
GNN	Graph neural network
HSA	Highest single agent
HTS	High-throughput screening
NLL	Negative log-likelihood
ZIP	Zero interaction potency

Notation

G	Graph
E	Edge set (bonds)
V	Node set (atoms)
R	Node set size (number of atoms)
A	Adjacency matrix
h_i	Atom feature vector
N_i	Atom neighbors
$a_{i,j}$	attention coefficients
L	Number of GNN layers
u	Drug or cell line input feature vector
$g^{(l)}$	Layer-specific graph representation vector
z	Drug or cell line representation vector
T	Number of genes
M	Number of samples
y	True label
\hat{y}	Predicted label

References

- [1] Avner, B.S., Fialho, A.M., Chakrabarty, A.M.: Overcoming drug resistance in multi-drug resistant cancers and microorganisms: A conceptual framework. *Bioengineered* 3(5), 262 (2012). doi:10.4161/BIOE.21130 2

- [2] Mokhtari, R.B., Homayouni, T.S., Baluch, N., Morgatskaya, E., Kumar, S., Das, B., Yeger, H., Mokhtari, R.B., Homayouni, T.S., Baluch, N., Morgatskaya, E., Kumar, S., Das, B., Yeger, H.: Combination therapy in combating cancer. *Oncotarget* **8**(23), 38022–38043 (2017). doi:10.18632/ONCOTARGET.16723 2
- [3] Holbeck, S.L., Camalier, R., Crowell, J.A., Govindharajulu, J.P., Hollingshead, M., Anderson, L.W., Polley, E., Rubinstein, L., Srivastava, A., Wilsker, D., *et al.*: The national cancer institute almanac: a comprehensive screening resource for the detection of anticancer drug pairs with enhanced therapeutic activity. *Cancer research* **77**(13), 3564–3576 (2017) 2, 3
- [4] Holbeck, S.L., Camalier, R., Crowell, J.A., Govindharajulu, J.P., Hollingshead, M., Anderson, L.W., Polley, E., Rubinstein, L., Srivastava, A., Wilsker, D., Collins, J.M., Doroshow, J.H.: The National Cancer Institute ALMANAC: A Comprehensive Screening Resource for the Detection of Anticancer Drug Pairs with Enhanced Therapeutic Activity. *Cancer research* **77**(13), 3564–3576 (2017). doi:10.1158/0008-5472.CAN-17-0489 2
- [5] O’Neil, J., Benita, Y., Feldman, I., Chenard, M., Roberts, B., Liu, Y., Li, J., Kral, A., Lejnine, S., Loboda, A., Arthur, W., Cristescu, R., Haines, B.B., Winter, C., Zhang, T., Bloecher, A., Shumway, S.D.: An Unbiased Oncology Compound Screen to Identify Novel Combination Strategies. *Molecular cancer therapeutics* **15**(6), 1155–1162 (2016). doi:10.1158/1535-7163.MCT-15-0843 2
- [6] Zheng, S., Aldahdooh, J., Shadbahr, T., Wang, Y., Aldahdooh, D., Bao, J., Wang, W., Tang, J.: Drugcomb update: a more comprehensive drug sensitivity data repository and analysis portal. *Nucleic acids research* **49**(W1), 174–184 (2021) 2, 3
- [7] Kumar, V., Dogra, N.: A Comprehensive Review on Deep Synergistic Drug Prediction Techniques for Cancer. *Archives of Computational Methods in Engineering* **1**, 1–19 (2021). doi:10.1007/S11831-021-09617-3/FIGURES/7 2
- [8] Preuer, K., Lewis, R.P.I., Hochreiter, S., Bender, A., Bulusu, K.C., Klambauer, G.: DeepSynergy: predicting anti-cancer drug synergy with Deep Learning. *Bioinformatics (Oxford, England)* **34**(9), 1538–1546 (2018). doi:10.1093/BIOINFORMATICS/BTX806 2, 7, 12
- [9] Zhang, T., Zhang, L., Payne, P.R., Li, F.: Synergistic drug combination prediction by integrating multiomics data in deep learning models. In: *Translational Bioinformatics for Therapeutic Development*, pp. 223–238. Springer, ??? (2021) 2, 12
- [10] Kuru, H.I., Tastan, O., Cicek, A.E.: MatchMaker: A Deep Learning Framework for Drug Synergy Prediction. *bioRxiv*, 2020–0524113241 (2020). doi:10.1101/2020.05.24.113241 2, 12
- [11] Wooten, J. D., Meyer, T. C., Lubbock, LR, A., Quaranta, Vito, Lopez, F. C.: Musyc is a consensus framework that unifies multi-drug synergy metrics for combinatorial drug discovery. *Nature communications* **12**(1), 1–16 (2021) 2, 4, 12
- [12] O’Neil, J., Benita, Y., Feldman, I., Chenard, M., Roberts, B., Liu, Y., Li, J., Kral, A., Lejnine, S., Loboda, A., *et al.*: An unbiased oncology compound screen to identify novel combination strategies. *Molecular cancer therapeutics* **15**(6), 1155–1162 (2016) 3
- [13] Licciardello, M.P., Ringler, A., Markt, P., Klepsch, F., Lardeau, C.-H., Sdelci, S., Schirghuber, E., Müller, A.C., Caldera, M., Wagner, A., *et al.*: A combinatorial screen of the cloud uncovers a synergy targeting the androgen receptor. *Nature chemical biology* **13**(7), 771–778 (2017) 3
- [14] Landrum, G.: Rdkit: open-source cheminformatics <http://www.rdkit.org>. Google Scholar There is no corresponding record for this reference (2016) 3, 8
- [15] Iorio, F., Knijnenburg, T.A., Vis, D.J., Bignell, G.R., Menden, M.P., Schubert, M., Aben, N., Gonçalves, E., Barthorpe, S., Lightfoot, H., *et al.*: A landscape of pharmacogenomic interactions in cancer. *Cell* **166**(3), 740–754 (2016) 3
- [16] Subramanian, A., Narayan, R., Corsello, S.M., Peck, D.D., Natoli, T.E., Lu, X., Gould, J., Davis, J.F., Tubelli, A.A., Asiedu, J.K., *et al.*: A next generation connectivity map: L1000 platform and the first 1,000,000 profiles. *Cell* **171**(6), 1437–1452 (2017) 3
- [17] Geary, N.: Understanding synergy. *American Journal of Physiology - Endocrinology and Metabolism* **304**(3), 237–253 (2013). doi:10.1152/AJPENDO.00308.2012/ASSET/IMAGES/LARGE/ZH10031367510010.JPEG 3
- [18] He, L., Kuleskiy, E., Saarela, J., Turunen, L., Wennerberg, K., Aittokallio, T., Tang, J.: Methods for high-throughput drug combination screening and synergy scoring. In: *Cancer Systems Biology*, pp. 351–398. Springer, ??? (2018) 4
- [19] Brody, S., Alon, U., Yahav, E.: How attentive are graph attention networks? *arXiv preprint arXiv:2105.14491* (2021) 5

- [20] Velickovic, P., Cucurull, G., Casanova, A., Romero, A., Lio, P., Bengio, Y.: Graph attention networks. *stat* **1050**, 20 (2017) 5
- [21] Pedregosa, F., Varoquaux, G., Gramfort, A., Michel, V., Thirion, B., Grisel, O., Blondel, M., Prettenhofer, P., Weiss, R., Dubourg, V., Vanderplas, J., Passos, A., Cournapeau, D., Brucher, M., Perrot, M., Duchesnay, E.: Scikit-learn: Machine learning in Python. *Journal of Machine Learning Research* **12**, 2825–2830 (2011) 7, 8
- [22] Fey, M., Lenssen, J.E.: Fast graph representation learning with pytorch geometric. *arXiv preprint arXiv:1903.02428* (2019) 8
- [23] Paszke, A., Gross, S., Chintala, S., Chanan, G., Yang, E., DeVito, Z., Lin, Z., Desmaison, A., Antiga, L., Lerer, A.: Automatic differentiation in PyTorch (2017). Accessed 2020-07-29 8
- [24] Hu, W., Fey, M., Zitnik, M., Dong, Y., Ren, H., Liu, B., Catasta, M., Leskovec, J.: Open graph benchmark: Datasets for machine learning on graphs. *Advances in neural information processing systems* **33**, 22118–22133 (2020) 8
- [25] Hu, W., Liu, B., Gomes, J., Zitnik, M., Liang, P., Pande, V., Leskovec, J.: Strategies for pre-training graph neural networks. In: *International Conference on Learning Representations* (2020). <https://openreview.net/forum?id=HJIWWJSFDH> 8

Supplementary Files

List of landmark genes

AARS, ABCC5, ABCF1, ABHD4, ABHD6, ABL1, ACAA1, ACAT2, ACBD3, ACD, ACLY, ACOT9, ADAM10, ADAT1, ADH5, ADI1, ADO, ADRB2, AGL, AKAP8, AKAP8L, AKR7A2, AKT1, ALAS1, ALDH7A1, ALDOA, AMDHD2, ANKRD10, ANO10, ANXA7, APBB2, APOE, APP, APPBP2, ARFP2, ARHGAP1, ARHGEF12, ARHGEF2, ARID4B, ARID5B, ARL4C, ARNT2, ARPP19, ASAH1, ASCC3, ATF1, ATF5, ATF6, ATG3, ATMIN, ATP11B, ATP1B1, ATP2C1, ATP6V0B, ATP6V1D, AURKA, AURKB, AXIN1, BACE2, BAD, BAG3, BAMB1, BAX, BCL2, BCL7B, BDH1, BECN1, BHLHE40, BID, BIRC2, BIRC5, BLCAP, BLMH, BLVRA, BMP4, BNIP3, BNIP3L, BPHL, BRCA1, BTK, BZW2, C2CD2, C2CD2L, C2CD5, C5, CAB39, CALM3, CALU, CAMSAP2, CANT1, CAPN1, CASC3, CASK, CASP10, CASP2, CASP3, CASP7, CAST, CAT, CBLB, CBR1, CBR3, CCDC85B, CCDC86, CCDC92, CCL2, CCNA1, CCNA2, CCNB1, CCND1, CCND3, CCNE2, CCNF, CCNH, CCP110, CD320, CD40, CD44, CDC20, CDC25A, CDC25B, CDC42, CDC45, CDCA4, CDH3, CDK1, CDK19, CDK2, CDK4, CDK5R1, CDK6, CDK7, CDKN1B, CDKN2A, CEBPD, CEBPZ, CENPE, CEP57, CERK, CETN3, CFLAR, CGRRF1, CHAC1, CHEK1, CHEK2, CHIC2, CHMP6, CHN1, CHP1, CIAPIN1, CIRBP, CISD1, CLIC4, CLPX, CLSTN1, CLTB, CLTC, CNDP2, CNOT4, CNPY3, COASY, COG2, COG4, COG7, COL1A1, COL4A1, COPB2, COPS7A, CORO1A, CPNE3, CPSF4, CREB1, CREG1, CRELD2, CRK, CRKL, CRTAP, CRYZ, CSK, CSNK1A1, CSNK1E, CSNK2A2, CSRP1, CTNNA1, CTNND1, CTTN, CXCL2, CXCR4, CYB561, CYTH1, DAG1, DAXX, DCK, DCTD, DCUN1D4, DDB2, DDT4, DDR1, DDX10, DDX42, DECR1, DENND2D, DERA, DFFA, DFFB, DHDDS, DHRS7, DHX29, DLD, DMTF1, DNAJA3, DNAJB1, DNAJB2, DNAJB6, DNAJC15, DNM1, DNM1L, DNMT1, DNMT3A, DNMTTIP2, DPH2, DRAP1, DSG2, DUSP11, DUSP14, DUSP22, DUSP3, DUSP4, DUSP6, DYNLT3, DYRK3, E2F2, EAPP, EBNA1BP2, EBP, ECD, ECHI, EDEM1, EDN1, EED, EFCAB14, EGF, EGFR, EGR1, EIF4EBP1, EIF5, ELAC2, ELAVL1, ELOVL6, EML3, ENOPH1, ENOSF1, EPB41L2, EPHA3, EPHB2, EPN2, EPRS, ERBB2, ERBB3, ETFB, ETS1, ETV1, EVL, EXOSC4, EXT1, EZH2, FAH, FAIM, FAM20B, FAM57A, FAM69A, FAS, FAT1, FBXL12, FBXO11, FBXO21, FBXO7, FCHO1, FDF1, FEZ2, FGFR2, FGFR4, FHL2, FIS1, FKBP14, FKBP4, FOS, FOSL1, FOXJ3, FOXO3, FOXO4, FPGS, FRS2, FSD1, FUT1, FYN, FZD1, FZD7, G3BP1, GAA, GABPB1, GADD45A, GADD45B, GALE, GAPDH, GATA2, GATA3, GPD5, GFOD1, GFPT1, GHR, GLI2, GLOD4, GLRX, GMNN, GNA11, GNA15, GNAI1, GNAI2, GNAS, GNB5, GNPDA1, GOLT1B, GPATCH8, GPC1, GRB10, GRB7, GRN, GRWD1, GSTZ1, GTF2A2, GTF2E2, GTPBP8, H2AFV, HADH, HAT1, HDAC2, HDAC6, HEATR1, HEBP1, HERC6, HERPUD1, HES1, HIST1H2BK, HIST2H2BE, HK1, HLA-DRA, HMG20B, HMG2, HMGCR, HMGCS1, HMOX1, HN1L, HOMER2, HOOK2, HPR1, HS2ST1, HSD17B10, HSPA1A, HSPA4, HSPA8, HSPD1, HTATS1, HTRA1, HYOU1, IARS2, ICAMI1, ICAM3, ICMT, ID2, IDE, IER3, IFNAR1, IFRD2, IGF1R, IGF2BP2, IGF2R, IGFBP3, IGHMBP2, IKBKAP, IKKB, IKBKE, IKZF1, IL13RA1, IL1B, IL4R, ILK, INPP1, INPP4B, INSI1, INTS3, IPO13, IQGAP1, ISOC1, ITFG1, ITGAE, ITGB1BP1, ITGB5, JMJD6, JUN, KAT6A, KAT6B, KCNK1, KCTD5, KDM3A, KDM5A, KDM5B, KEAP1, KIAA0100, KIAA0355, KIAA0753, KIAA0907, KIF14, KIF20A, KIF2C, KIF5C, KIT, KLHDC2, KLHL21, KLHL9, KTN1, LAGE3, LAMA3, LAP3, LBR, LGALS8, LGMN, LIG1, LIPA, LOXL1, LPAR2, LPGAT1, LRP10, LRPAP1, LRRC41, LSM5, LSM6, LSR, LYN, LYRM1, MACF1, MALT1, MAMLD1, MAN2B1, MAP2K5, MAP3K4, MAP4K4, MAP7, MAPK13, MAPK11P1L, MAPK9, MAPKAPK2, MAPKAPK3, MAPKAPK5, MAST2, MAT2A, MBNL1, MBNL2, MBOAT7, MBTPS1, MCM3, MCOLN1, ME2, MEF2C, MELK, MEST, MFSD10, MICALL1, MIF, MKNK1, MLEC, MILLT1, MMP1, MMP2, MOK, MPC2, MPZL1, MRPL19, MRPS16, MRPS2, MSH6, MSRA, MTA1, MTF2, MTFR1, MTHFD2, MUC1, MVP, MYBL2, MYC, MYCBP, MYCBP2, MYL9, MYLK, MYO10, NARFL, NCAPD2, NCK2, NCOA3, NENF, NET1, NFATC3, NFATC4, NFE2L2, NFIL3, NFKB2, NFKBIA, NFKBIB, NFKBIE, NIPSNAP1, NISCH, NIT1, NMT1, NNT, NOL3, NOLC1, NOS3, NOSIP, NOTCH1, NPC1, NPDC1, NPEPL1, NPRL2, NR1H2, NR2F6, NR3C1, NRAS, NRIP1, NSDHL, NTSDC2, NUCB2, NUDCD3, NUDT9, NUP133, NUP85, NUP88, NUP93, NUSAP1, NVL, ORC1, OXA1L, OXCT1, OXSR1, P4HA2, P4HTM, PACSIN3, PAF1, PAFAH1B1, PAFAH1B3, PAICS, PAK1, PAK4, PAK6, PAN2, PAPP7, PARP1, PARP2, PAX8, PCBD1, PCCB, PCK2, PCMI, PCMT1, PCNA, PDGFA, PDHX, PDIA5, PDLIM1, PDS5A, PECR, PEX11A, PFKL, PGM1, PGRMC1, PHGDH, PHKA1, PHKB, PHKG2, PIGB, PIH1D1, PIK3C2B, PIK3C3, PIK3CA, PIK3R3, PIK3R4, PIN1, PIP4K2B, PKIG, PLA2G15, PLA2G4A, PLCB3, PLEKHJ1, PLEKHM1, PLK1, PLOD3, PLP2, PLS1, PLSCR1, PMAIP1, PMM2, PNP, PNP, POLB, POLE2, POLG2, POLR1C, POLR21, POLR2K, POPA, PPARG, PPARG, PPIC, PPIE, PPOX, PPP1R13B, PPP2R3C, PPP2R5A, PPP2R5E, PRAF2, PRCP, PRKACA, PRKAG2, PRKCD, PRKCQ, PRKX, PROS1, PRPF4, PRR15L, PRR7, PRSS23, PSIP1, PSMB8, PSDM10, PSDM4, PSME1, PSMF1, PSMG1, PSRC1, PTGS2, PTK2, PTK2B, PTPN1, PTPN12, PTPN6, PTPRC, PTPRE, PTPRK, PUF60, PWP1, PXN, PYCR1, PYGL, RAB11FIP2, RAB21, RAB27A, RAB31, RAB4A, RAD51C, RAD9A, RAE1, RAI14, RALA, RALB, RALGDS, RAPIGAP, RAS1, RB1, RBKS, RBM15B, RBM6, REEP5, RELB, RFC2, RFC5, RFNG, RFX5, RGS2, RHEB, RHOA, RNF167, RNH1, RNMT, RNPS1, RPA1, RPA2, RPA3, RPIA, RPL39L, RPN1, RPS5, RPS6, RPS6KA1, RRAGA, RRP12, RRP1B, RRP8, RRS1, RSU1, RTN2, RUVBL1, S100A13, S100A4, SACM1L, SCAND1, SCARB1, SCCPDH, SCP2, SCRNI, SCYL3, SDHB, SENP6, SERPINE1, SESN1, SFN, SGCB, SH3BP5, SHC1, SIRT3, SKIV2L, SKP1, SLC11A2, SLC1A4, SLC25A13, SLC25A14, SLC25A4, SLC25A46, SLC27A3, SLC2A6, SLC35A1, SLC35A3, SLC35B1, SLC35F2, SLC37A4, SLC5A6, SMAD3, SMARCA4, SMARCC1, SMARCD2, SMC1A, SMC3, SMC4, SMNDC1, SNAP25, SNCA, SNX11, SNX13, SNX6, SNX7, SOCS2, SORBS3, SOX4, SPAG4, SPAG7, SPDEF, SPEN, SPP1, SPR, SPRED2, SPTAN1, SPTLC2, SQRLD, SQSTM1, SRC, SSBP2, ST3GAL5, ST6GALNAC2, ST7, STAMBP, STAP2, STAT1, STAT3, STAT5B, STK10, STK25, STMN1, STX1A, STX4, STXB1, STXB2, SUPV3L1, SUV39H1, SUZ12, SYK, SYNE2, SYNGR3, SYPL1, TARBPI1, TATDN2, TBC1D9B, TBP, TBPL1, TBX2, TBXA2R, TCEA2, TCEAL4, TCERG1, TCFL5, TCTA, TCTN1, TERF2IP, TERT, TES, TESK1, TEX10, TFAP2A, TFD1, TGFβ3, TGFβR2, THAP11, TIAM1, TICAM1, TIMELESS, TIMM17B, TIMM22, TIMM9, TIMP2, TIPARP, TIJ1, TLE1, TLK2, TLR4, TM9SF2, TM9SF3, TMCO1, TMED10, TMEM109, TMEM2, TMEM5, TMEM50A, TMEM97, TNFRSF21, TNIP1, TOMM34, TOP2A, TOPBP1, TOR1A, TP53, TP53BP1, TP53BP2, TP53L2, TPM1, TRAK2, TRAM2, TRAP1, TRAPPC3, TRAPPC6A, TRIB1, TRIB3, TRIM13, TRIM2, TSC22D3, TSEN2, TSKU, TSPAN3, TSPAN4, TSPAN6, TSTA3, TUBB6, TXLNA, TXNDC9, TXNL4B, TXNRD1, UBE2A, UBE2C, UBE2J1, UBE2L6, UBE3B, UBE3C, UBQLN2, UBR7, UFM1, UGDH, USP1, USP14, USP22, USP6NL, USP7, UTP14A, VAPB, VAT1, VAV3, VGLL4, VPS28, VPS72, WAF3F, WDR61, WDR7, WDTC1, WFS1, WIPF2, WRB, XBP1, XPNPEP1, XPO7, YKT6, YME1L1, YTHDF1, ZDHHC6, ZFP36, ZMIZ1, ZMYM2, ZNF131, ZNF274, ZNF318, ZNF395, ZNF451, ZNF586, ZNF589